Biomaterials Science

ROYAL SOCIETY OF CHEMISTRY

PAPER

View Article Online
View Journal

Cite this: DOI: 10.1039/d1bm00711d

In situ gelling and dissolvable hydrogels for use as on-demand wound dressings for burns†

Katherine A. Cook,[a] Nada Naguib,[a] Jack Kirsch,[a] Katherine Hohl,[a,b] Aaron H. Colby,[a] Robert Sheridan,[c] Edward K. Rodriguez,[b] Ara Nazarian[b] and Mark W. Grinstaff *[a]

Received 7th May 2021,
Accepted 5th August 2021

DOI: 10.1039/d1bm00711d

rsc.li/biomaterials-science

Currently, no dressings utilized in burn clinics provide adhesion, hydration or mechanical strength on the same order as human skin as well as the ability to be atraumatically removed. We report the synthesis, characterization, and *in vivo* evaluation of *in situ* polymerized and subsequent dissolvable hydrogels as burn wound dressings. Hydrogel dressings, from a small library of synthesized materials form *in situ*, exhibit storage moduli between 100–40 000 Pa, dissolve on-demand within 10 minutes to 90 minutes, swell up to 350%, and adhere to both burned and healthy human skin at 0.2–0.3 N cm^{-2}. Further, results from an *in vivo* porcine second degree burn model demonstrate functional performance with healing equivalent to conventional treatments with the added benefit of facile, *in situ* application and subsequent removal *via* dissolution.

Introduction

According to the world health organization, approximately 11 million people require medical attention due to burns each year.[1] In low-income countries, burns cause nearly 200 000 deaths annually.[1] Within higher income countries, such as the United States, there are approximately 2 million fires, with 1.2 million people sustaining burn injuries.[2] Death rates are as high as 75% for patients with burn wounds on 40% or more of their body surface area due to infection, dehydration, and pain.[2] The greater the surface area of burns, the more serious the burn, such that a burn covering 15% or more of the total body surface area (TBSA) in adults requires hospitalization while only a 10% TBSA necessitates hospitalization in children.[1,3–9] Even when patients survive and recover from their injuries, many burn survivors must manage life-long disabilities and psychological trauma due to burns.[2,4,5,10] A second degree burn results in damage to both the epidermis and dermis layers of tissue, and is a challenging wound to manage due to inflammation, fluid loss, tissue damage, and loss of barrier function by the tissue.[11] Today, treatments for second degree burn wounds include antibiotics, fluid replacement, debridement (if necrotic), and dressings.[9,12,13] Wound healing is an evolving process that takes place over days to months depending on the size and severity of the burn, and dressings can be applied and replaced as many as 1–2 times per day in order to contain and remove the discharge of wound exudate.[7] These dressing changes require significant time (57 ± 34 min) and multiple personnel.[3] In addition to lengthy dressing changes, the act of dressing replacement often requires mechanical debridement and cutting, which traumatizes new tissue, affords longer healing times, and causes pain.[2–5,7,8,10,14–16] In fact, the pain can be severe enough to require anesthesia.[3,4,17] To address the unmet need for alternative and facile methods to replace a dressing for the management of second degree burns, we recently introduced the concept of a dissolvable hydrogel dressing.[18] Hydrogels are three-dimensional, hydrophilic networks used for a variety of biomedical applications such as tissue engineering, drug delivery, and wound management.[5,19–27] The two-part hydrogel dressing, described herein, forms *in situ* when mixed and applied to the wound as an aqueous solution or spray. Once applied, this dressing adheres and protects the tissue. To remove the dressing, an aqueous cysteine methyl ester (CME) solution is applied which selectively cleaves the internal covalent thioester linkages within the dressing. With a mindset towards translation, we report the synthesis of a small library of hydrogels, their physical and mechanical properties, and performance of an optimized hydrogel dressing in a large animal, second degree burn, pig model. Specifically, a poly

[a]*Departments of Chemistry, Biomedical Engineering, and Medicine, Boston University, Boston, MA 02215, USA. E-mail: mgrin@bu.edu*
[b]*Department of Surgery, Beth Israel Deaconess Medical Center, Boston, MA 02215, USA*
[c]*Shriners Hospitals for Children and Burns Service, Department of Surgery, Massachusetts General Hospital, Boston, MA, 02214, USA*

†Electronic supplementary information (ESI) available: Synthesis and characterization of materials, NMR spectra, MALDI spectra, kinetics studies, rheology, swelling, dissolution, and *in vivo* porcine study. See DOI: 10.1039/d1bm00711d

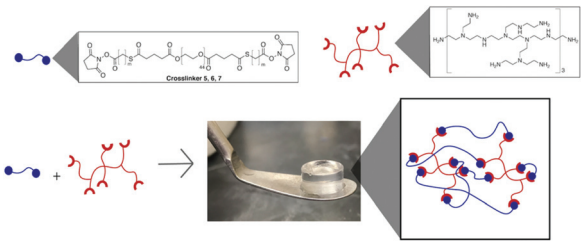

Fig. 1 Preparation of a three-dimensional hydrogel *via* the reaction between a poly(ethyleneimine) (PEI) and a NHS activated poly(ethylene glycol) (PEG) crosslinker.

(ethyleneimine) (PEI) crosslinks with a NHS activated poly (ethylene glycol) (PEG) containing internal thioester linkages to form an amide-crosslinked linked hydrogel (Fig. 1). The hydrogel dressing is applied *via* a syringe to the wound and removed by dissolution utilizing thiol-thioester exchange chemistry upon exposure to CME solution.

Results and discussion

Current burn dressings include gauze dressings, hydrocolloid dressings, silver-impregnated dressings, and hydrogel dressings.[8,28] With regards to wound dressing design and composition, our work focuses on developing hydrogel-based dressings. Hydrogels are ideal burn wound dressing materials as they protect the wound from the outside environment, absorb wound exudates, and possess mechanical properties and elasticity on the same order as that of epithelial tissue.[16,18,28–34] Specifically, we are investigating synthetic hydrogel dressings that form *in situ via* a reaction between an amine terminated, branched poly(ethyleneimine) (PEI) and a difunctionalized, NHS activated poly(ethylene glycol) (PEG) crosslinker (Fig. 1). Unique to the dressing design is an internal thioester linkage within the crosslinker which, in the presence of a cysteine methyl ester (CME), undergoes a thiol-thioester exchange to cleave the crosslinker and dissolve the dressing (Scheme 1). Herein, we vary the length of methylenes in the crosslinker from 1 to 5 to 10 in order to tune the physical and mechanical properties of the hydrogels, and to identify a hydrogel dressing formulation suitable for evaluation in a large animal porcine second degree burn model.

We synthesized crosslinkers **5**–**7** starting from PEG (M_w 3000) as shown in Scheme 2. Crosslinker **5** was previously synthesized and we adapted this procedure with minor modifications (Scheme 2).[35] Briefly, we reacted the starting PEG (M_w 3000) with the appropriate anhydride to form the PEG diacid and subsequently activated it with an NHS ester to give the crosslinker **1**. Crosslinker **1** was reacted with DBU, and the respective thiol-terminal carboxylic acids of 1, 5, and 10 methylenes, to afford intermediates **2**, **3**, and **4**, respectively. Next, we prepared the NHS-activated crosslinkers *via* DCC coupling chemistry with NHS and purified the products by precipitation in diethyl ether. The yields were high (85–98%) for all of the reactions. We characterized and confirmed the structure of the crosslinkers by ^{1}H NMR, ^{13}C NMR, GPC, MALDI and DSC, and the data is provided in the ESI (Fig. S1–S9).†

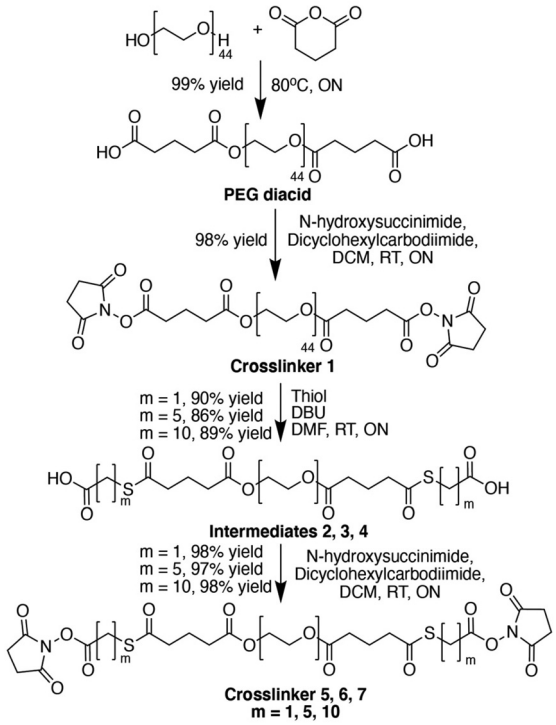

Scheme 2 Synthetic scheme of crosslinkers and intermediates **1**–**7**.

Next, we prepared a small library of 10, 15, and 20 wt% hydrogels by mixing the crosslinker, dissolved in 0.1 M phosphate buffer pH 6.5, with branched polyethyleneimine (PEI; M_w 1800) in 0.3 M borate buffer, pH 8.5. However, we observed minimal solubility of crosslinker **7** in buffer due to the hydrophobicity of the methylene chains. In order to overcome the low solubility, we dissolved crosslinker **7** in 0.1 M phosphate buffer pH 6.5 with 50% ethanol prior to mixing it with the PEI solution. The ratio of NHS : NH_2 was 2 : 1 to ensure amidation of PEI and the crosslinker. We observed no major difference in

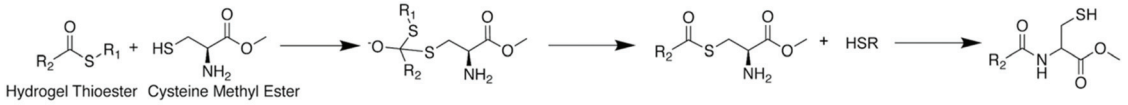

Scheme 1 Controlled dissolution through thiol-thioester exchange.

hydrogel mechanical properties with a 2 : 1 or 1 : 1 NHS : NH_2 ratio (Fig. S18 in ESI†). A transparent, solid hydrogel forms within 5 minutes for all compositions as determined by the inverted tube gelation test. Hydrogel gelation time positively correlates with increasing hydrophobic chain lengths. The hydrogel formulation with crosslinkers **5**, **6**, and **7** gel in less than 5 seconds, 90s, and 3–5 minutes, respectively (Fig. 3A). Gelation time also positively correlates with weight percent, the higher the weight percent the longer the gelation time.

Next, we characterized the morphology of the hydrogels using scanning electron microscopy (SEM). All of the hydrogels possess pore sizes varying from 5 μm to 100 μm with a honeycomb-like structure. Interestingly, the hydrogel prepared with **7**, unlike all the other hydrogels, exhibits a more lamellar-like structure (Fig. 2). Because of this observed secondary structure, we assessed the critical aggregation concentration (CAC) of crosslinker **7** using the pyrene assay. We observe a CAC of 0.050 mM, a concentration below that of our hydrogel crosslinker concentration indicating that we are likely forming a self-assembled structure within the hydrogel itself giving rise to the lamellar structure seen under SEM.

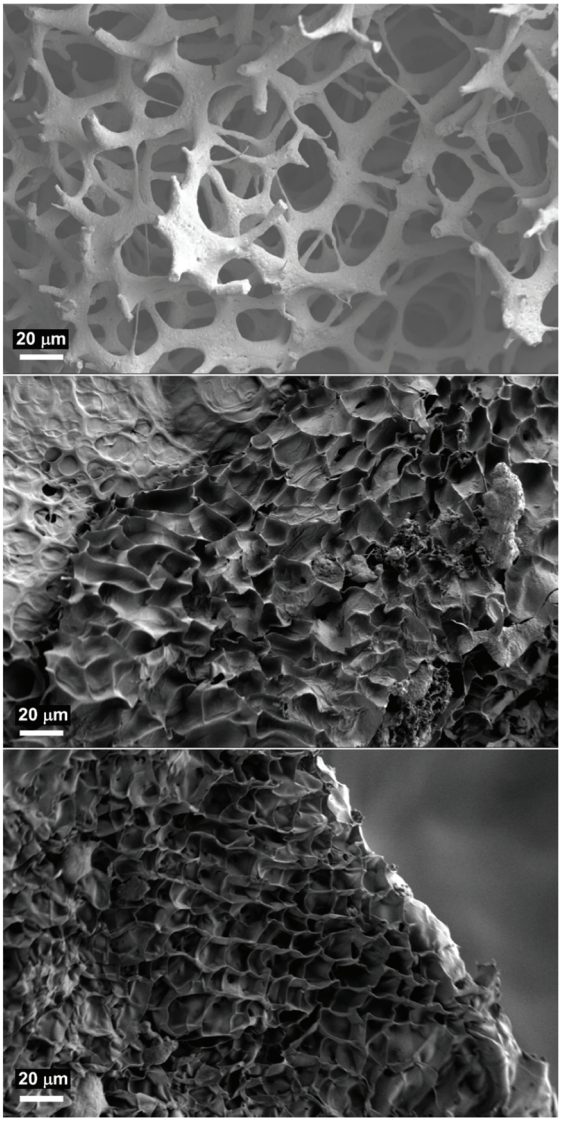

Fig. 2 SEM images of 5 (top) 6 (middle) and 7 (bottom).

From a chemical reactivity perspective, the terminal amines of the PEI may react with the terminal NHS ester or the internal thioesters to form an amide bond. Thus, we determined the preferential attack site for the amines *via* ^{1}H NMR using a model system. Specifically, we used *N*-butylamine, as a model of a primary terminal amine on PEI, and added it to an aqueous solution containing **6** and followed the amidation reaction *via* ^{1}H NMR. A selective reaction occurs between the amine and the NHS ester on the crosslinkers, and not the internal thiolester over 20 minutes (>99% at the NHS site). An upfield shift from the conjugated NHS ester at 2.82 ppm to free NHS at 2.49 ppm on crosslinker **6** (Fig. S10 in ESI†) confirms amidation at the NHS ester while the methylene peak at 2.6 ppm for the thioester does not shift. The attack of the terminal amine to the NHS-ester occurs quickly, under 10 seconds, however in hydrogels this reaction is likely slower because once one of the amines attacks the NHS-ester, entanglement and solidification occurs with a resulting increase in steric hindrance. Hence the lengthier gelation times. Additionally, a competitive hydrolysis reaction occurs at the NHS ester. Hydrolysis of the NHS ester, however, is negligible at pH 6.5 over twenty minutes, a longer time than necessary to form the hydrogel (Fig. S12C in ESI†). This selectivity of amidation at the NHS ester ensures that we retain the internal thioester linkage, allowing for subsequent dissolution through CME.

With regards to mechanical properties, we performed strain and frequency sweeps at various time points before and after swelling in 50 mM PBS. First, we determined the linear viscoelastic region using the strain sweep (Fig. S13 (left) in ESI†). We also performed a frequency sweep on all hydrogels with 3% strain from 1 to 10 Hz (Fig. S13 (right) in ESI†). These hydrogels exhibit viscoelastic, solid-like behavior, with the storage modulus (G') > loss modulus (G'').[36,37]

Over 30 days of swelling, we observed the lowest storage modulus with hydrogel **5**, sustaining a G' of below 10 kPa for the duration of time after swelling. The storage modulus of hydrogels composed of crosslinkers **6** and **7** are each larger (Fig. 3B), and at 15 wt% the storage moduli are approximately 12 kPa and 20 kPa, respectively (Fig. 3C). We attribute this increase in storage modulus in each hydrogel to the hydrophobicity of methylenes, such that the longer the methylene chain length, the greater the hydrophobic interactions and a stronger hydrogel. This observation holds true for the weight percent dependence. The higher the weight percent, the greater the storage modulus.

To ensure that the presence of ethanol does not increase the storage modulus for hydrogels prepared with crosslinker **7**, we assessed the rheological measurements of hydrogels prepared with crosslinker **6** under the same conditions as those hydrogels used for crosslinker **7**. We observed no significant

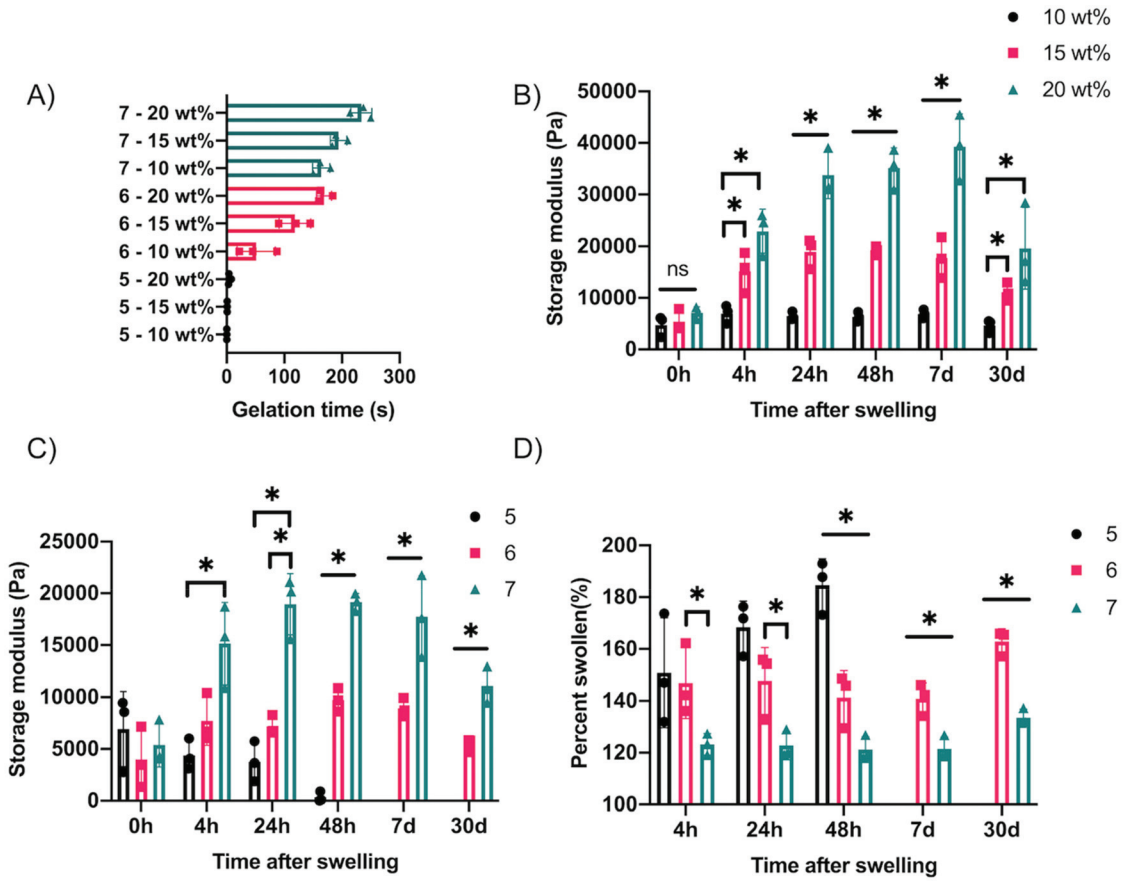

Fig. 3 (A) Gelation times of hydrogels at 10, 15 and 20 wt%. (B) Hydrogel 7 storage moduli at 10, 15 and 20 wt%. (C) Storage moduli of hydrogels **5**, **6**, and **7** at 15 wt%. (D) Swelling of hydrogels **5**, **6**, and **7** at 15 wt% over time. Storage moduli and swelling data for the 10 and 20 wt% hydrogels are found in the ESI.†

difference in storage modulus between hydrogels prepared with or without EtOH, indicating that the buffer conditions do not alter mechanical properties of our hydrogels (Fig. S19 in ESI†).

During the 30 days of swelling, the hydrogels swell between 150–350% depending on weight percent and hydrophobicity of the hydrogel formulation (Fig. 3D and S16 (left and right) in ESI†). Swelling reaches equilibrium after 48 hours for all formulations. Hydrogels with crosslinker **7** swell the least, likely as a consequence of the hydrophobicity within the long methylene chain length, while hydrogels with crosslinker **5** swell the most.

All of the hydrogels undergo hydrolysis over 30 days of swelling as indicated by a loss of gross structure and a reduction in storage modulus overtime (Fig. 3B and C). Hydrogel **5** exhibits an immediate loss in storage modulus and gross structure while hydrogels **6** and **7** initially increase in strength as they swell. However, we ultimately observe a reduction in storage modulus in hydrogels **6** and **7** by 30 days post swelling. We attribute this loss in structure and mechanical properties to hydrolysis of the crosslinker. To further characterize the hydrolysis, we measured the rate of crosslinker hydrolysis in 0.1 M sodium bicarbonate buffer, pH 8.0, *via* ^{1}H NMR. Hydrolysis preferentially occurs at the thioester linkage with a rate of $k = 0.055$ min^{-1} and $k = 0.003$ min^{-1} for crosslinkers **5** and **6**, respectively (Fig. S12A and B in ESI†) as opposed to the ester linkage between the glutaric acid and PEG on the crosslinker. **7** is stable for over 7 days. We attribute the stability of the thioester linkage in crosslinker **7** to the hydrophobic methylene chain length protecting the adjacent thioester from hydrolysis (Scheme 3).

Aside from hydrolysis, the thioester facilitates hydrogel dissolution through thiol-thioester exchange in the presence of cysteine methyl ester (CME).[18] Upon exposure of the dressing to a 0.3 M CME solution at pH 8.6, the thiol on the cysteine methyl ester attacks and displaces the internal thioester in the crosslinker. The amine on the now internal cysteine methyl ester subsequently rearranges to form an amide bond by replacing the thioester (Scheme 1). This amide bond prevents reattack of the original, internal thiol (Schemes 1 and 3). This dissolution process fragments the hydrogel network, degrading the hydrogel over time. Thus, we assessed the storage modulus of the hydrogel in a CME solution as a function of time at pH 8.6. Loss of hydrogel structure, defined by $G' < 300$

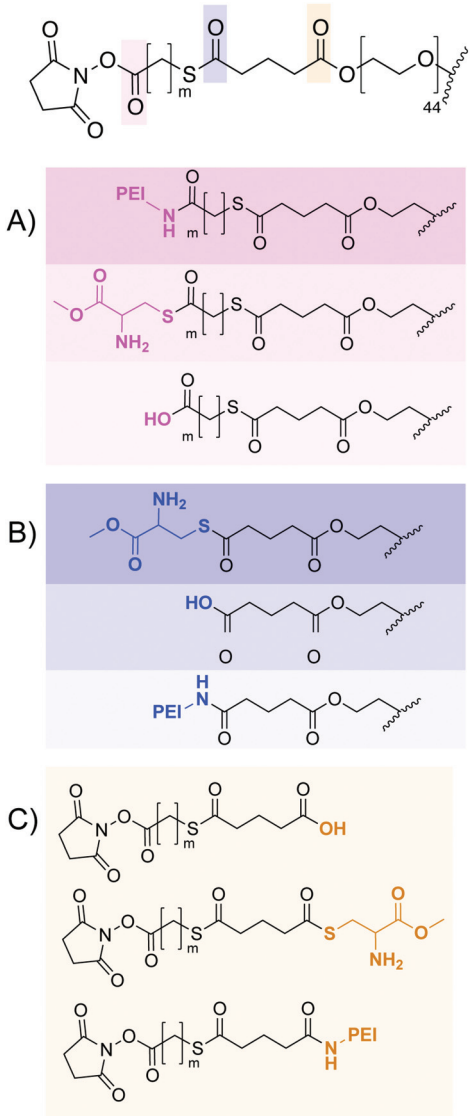

Scheme 3 Selective conjugation of the crosslinker with PEI, cysteine methyl ester, and water. (A) Reaction with the NHS ester. (B) Reaction with the internal thioester. (C) Reaction with the internal ester. Darker colored region corresponds with greater reactivity.

Pa, occurs in less than 10 minutes to over 90 minutes depending on the hydrogel formulation and weight percent, with a higher weight percent and longer methylene chain length resulting in an increase in time to dissolution (Fig. 4A and S17 (left and right) in ESI†). Specifically, at 15 wt%, hydrogel **5** dissolves within 10 minutes, while hydrogel **6** dissolves within 30 minutes and gel **7** dissolves within 80 minutes. This trend continues throughout all hydrogels regardless of weight percent. We accredit the slower dissolution of hydrogel **7** to the additional hydrophobic methylenes near the thioester decreasing the local hydrophilicity compared to **5** and **6**. Due to a competitive reaction at the thioester between hydrolysis of water and thiol-thioester exchange, we investigated the rate of dissolution using CME in sodium bicarbonate buffer pH 8.0 *via* ^{1}H NMR with crosslinker **6** (Scheme 3). We monitored the decrease in the methylene proton adjacent to the thioester and determined the thiol-thioester exchange rate to be k = 0.084 min^{-1}. This rate is faster than that of hydrolysis and, therefore, indicates that thiol-thioester exchange is the preferred mode of dissolution under 0.3 M CME solution conditions.

To investigate the applicability of our hydrogels as burn wound dressings, we assessed their adhesive properties against human skin. We performed a lap shear test to determine adhesion strength on *ex vivo* human breast and abdominal tissue. All the hydrogels adhere similarly to tissue with values of approximately 0.5 N cm^{-2} and display cohesive failure at the hydrogel-skin interface (Fig. 4B and C). Additionally, the hydrogel adheres similarly to burned skin as well as healthy skin. We attribute the adhesive strength to physical entanglement between the hydrogel and the human skin. The hydrogel, applied *in situ* as a liquid, allows for gelation to occur and take on the morphology of the human skin creating entanglements between the hydrogel and the skin. These hydrogels exhibit lower strength as compared to that of fibrin glue (0.6 ± 0.04 N cm^{-2}).[38] The hydrogels possess a favorable characteristic that enables their use on damaged soft tissues that are too weak for significant mechanical agitation or debridement.

Prior to the *in vivo* studies, we assessed cytotoxicity using NIH3T3 fibroblasts. Hydrogels **6** and **7** show >85% viability while **5** shows very low viability due to the rapid release of glutaric acid and increase in local acidity from the dissolution (Fig. S20 in ESI†).

Based on the sum of these results, we selected hydrogel **6** at 15 wt% for *in vivo* testing. Specifically, hydrogel **6** exhibits minimal cytotoxicity, possesses a storage modulus on the same order as that of human skin, maintains its mechanical strength and structure over 7 days' time, adheres to skin, swells, and dissolves in 30 minutes. For the *in vivo* model, we induced second-degree burns on four pigs by heating a brass cylinder (4 cm diameter) to 80 °C and placing it on the back of the pig for 20 seconds (12 wounds on a single pig; approximately 0.4% of the entire pig skin surface). We assessed the treatment groups at days 7 and 14, with one or two dressing changes as depicted in Fig. 5 and 6 to observe any differences in healing between groups. Specifically, we compared hydrogel **6** with commercially available gauze sponge dressing, Mepilex™, and xeroform. Triple antibiotic ointment was applied to each burn prior to dressing. Post-necropsy, the tissue was dissected, stained with H&E, and analysed (Fig. S21–S25, and Tables S1–S5 in ESI†).

Generally, all treatment groups show mild/moderate necrosis, epidermal ulceration, inflammation, and neovascularization. While the differences between the groups are not statistically significant, (P > 0.05), hydrogel **6** trends towards better performance over conventional gauze, Mepilex™, and xeroform dressings. Use of hydrogel **6** affords a trend towards less necrosis, epidermal ulceration, and inflammation compared to the other treatment groups, with similar neovascularization,

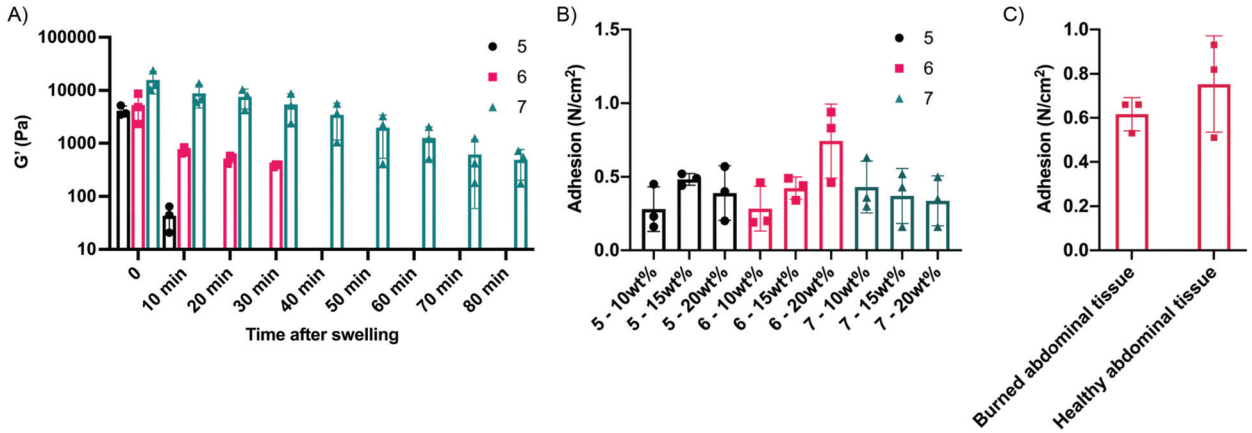

Fig. 4 (A) Dissolution of hydrogels at 15 wt% in 0.3 M CME solution. (B) Adhesion of hydrogels on human breast tissue using a lap shear test. (C) Adhesion of 15 wt% hydrogel 6 on burned and unburned human abdominal tissue.

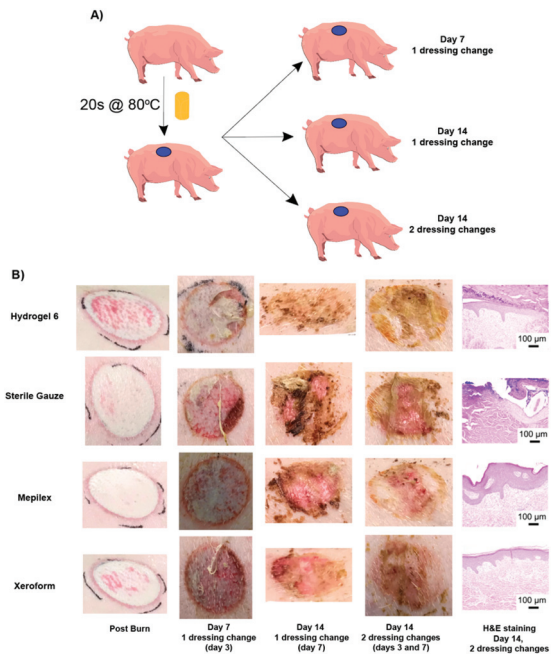

Fig. 5 *In vivo* porcine study (A) and burn sites at varying time points between dressing changes including end H&E staining of burn tissue (B).

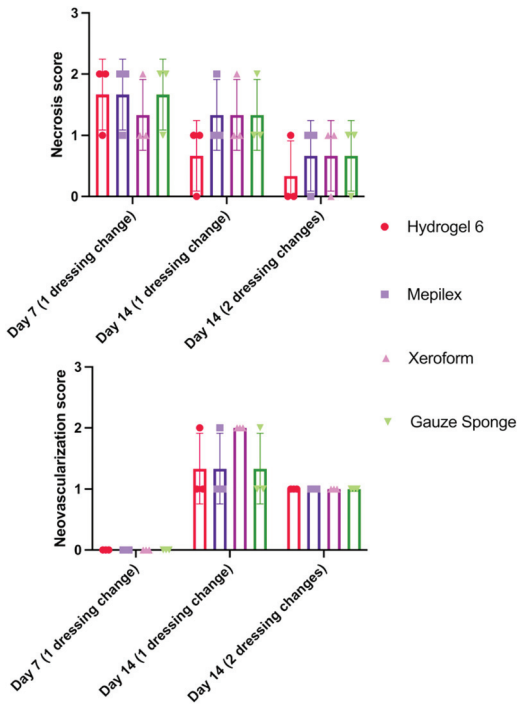

Fig. 6 Histopathology scores from the *in vivo* porcine study assessing necrosis (top) and neovascularization (bottom).

and burn depth (mm) and epidermal dermal thickness (mm) to all treatment groups by day 14 (Fig. 6). Additionally, all hydrogels show some re-epithelialization by day 14, with hydrogel **6** exhibiting complete re-epithelialization on two burns, and partial re-epithelialization on one ($N = 3$) after two dressing changes; the only dressing with more than one complete re-epithelialized burn. Of the other treatment groups, only the sterile gauze dressing on day 14, with two dressing changes, affords complete re-epithelialization. The spray-on application and removal process of our hydrogels allows for facile dressing changes, and eliminates the need for mechanical debridement and disruption of newly formed tissue.

Experimental

Materials

NMR spectra were recorded on a Varian 500 MHz VNMRs instrument; chemical shifts are quoted in parts per million (ppm) calibrated to residual non-deuterated solvent (^{1}H NMR: $CDCl_3$ at 7.26 ppm; ^{13}C NMR: $CDCl_3$ at 77.16 ppm). Coupling constants (J) are quoted in Hertz. Multiplicities are given as: singlet(s), doublet(d), triplet(t), quartet(q), multiplet(m) or broad(br). Gel permeation chromatography (GPC) was used to determine molecular weight and polymeric distribution in

tetrahydrofuran (THF) as the mobile phase with flow rate of 1.0 mL min^{-1}. GPC experiments were obtained using an OptiLab DSP Interferometric Refractometer (Wyatt Technology) fitted with two identical Jordi Gel DVB columns (Jordi Labs, 250 mm × 10 mm, 105 Å pore size). Matrix-assisted laser desorption/ionization (MALDI) mass spectra were recorded on a Bruker autoflex Speed MALDI-TOF spectrometer. Positive ion mass spectra were acquired in linear mode. Alpha-cyano-4-hydroxycinnamic acid solution in acetonitrile and water (3 : 1, 10 mg mL^{-1}) was used as a matrix. 8–12 mg of crosslinkers were mixed in 1 mL of 3 : 1 ACN : H_2O solution and 0.5 μL of the crosslinker matrix solution were each deposited on a MALDI plate layered as matrix : crosslinker : matrix solution. Differential scanning calorimetry (DSC) of crosslinkers were recorded on a DSC Q100 TA instrument.

All anhydrous solvents were purchased from Sigma Aldrich. All reagents were purchased from commercial sources and used without further purification. All reactions were carried out under argon with magnetic stirring. Polyethyleneimine, molecular weight 2000, was purchased from Polysciences, Inc.

Synthesis and characterization of compounds

The synthesis of the macromers is described in the SI along with the characterization data to include ^{1}H NMR, ^{13}C NMR, GPC, and MALDI-TOF data.

Mechanical properties of hydrogels

The rheological measurements were obtained from TA Instruments DHR-2 Rheometer. To prepare the hydrogels, PEI in borate buffer with pH adjusted to 8.5 with HCl was reacted with crosslinker **5**, **6**, or **7**, of 3400 MW (NHS-PEG-NHS) in phosphate buffer, pH 6.0. The ratio of amine to NHS was 1 : 15, and the concentration of the hydrogel was 10, 15, or 20 wt%. Crosslinker **5** formed a hydrogel instantaneously in under 5 seconds, while crosslinkers **6** and **7** formed hydrogels in 3 to 5 minutes at room temperature. Hydrogels with 8 mm width and 2.5 mm height were prepared in a cylindrical, Teflon mold and analyzed after sitting in a humid chamber for 1 hour at room temperature, 25 °C. The frequency sweeps were measured between 0.1 Hz and 10 Hz with an oscillatory strain percent of 3% and a temperature of 22 °C. An axial force of 0.15N was applied to the hydrogel using 8 mm parallel plate geometry. The oscillatory strain sweeps were recorded at a frequency of 0.1 Hz. Data are expressed as mean ± standard deviation (n = 3).

The adhesion of hydrogels between two pieces of human breast tissue at 10, 15 and 20 wt% was determined using an Instron 5944 Micro-tester. Hydrogels were prepared as mentioned above and injected between two pieces of human breast tissue. Hydrogels were left to gel for 1 hour at room temperature. After one hour, a lap shear test following ASTM D3165 protocol adhesion of the hydrogels on human tissue. Tissue pieces were pulled apart at a rate of 5 mm min^{-1} at room temperature until a break in adhesion was detected and recorded. Data are expressed as mean ± standard deviation (n = 3). Human abdominal skin and breast tissue was obtained from Massachusetts General Hospital (MGH IRB #2015P001267 for discarded, deidentified tissue).

The kinetics of gelation for hydrogels at all weight percents was determined by the inverted tube test. Gels were formed in glass vials and gelation was determined when the gel no longer runs down the sides of the vial when inverted. Data are expressed as mean ± standard deviation (n = 3). At the beginning of the experiment, solutions of crosslinkers and dendrons mixed together were liquid as gelation had just begun. The hydrogels became more viscoelastic and were solid at the end of the experiment.

Swelling ratio was determined by submerging and weighing the hydrogels in 3 mL of 100 mM PBS at pH 7.4 over 30 days. At time 0 h, 4 h, 24 h, 48 h, 7d, and 30d, the hydrogel was weighed. Swelling ratio is the percentage that the hydrogel swells, determined by

$$\text{Swelling ratio} = \frac{\text{final mass}}{\text{initial mass}} \times 100.$$

Final mass is the mass of the hydrogel at each time point after swelling. Initial mass is the mass of the hydrogel at time 0 h.

The solvent system used for the hydrogel formation kinetics study was 0.5 mL of $CDCl_3$. Crosslinker **6** was dissolved in this system. An initial ^{1}H NMR spectrum was taken and subsequently 2.0 eq. of *N*-butylamine was added to the NMR tube and an additional ^{1}H NMR spectrum was taken. Hydrolysis kinetics systems used 0.5 mL of D_2O and 10 mg Sodium bicarbonate, pH 8.0 as the solvent system. Crosslinkers **5** and **6** were each dissolved in the solvent system and ^{1}H NMR was used to follow hydrolysis overtime. The concentration *vs.* time was plotted and a non-linear regression was fitted to the curve. The rate constant, k, was calculated using the first order rate law equation: $[A] = [A]_o e^{-kt}$.

In vivo porcine burn model

All animal procedures were performed in accordance with the Guidelines for Care and Use of Laboratory Animals of CBSET and approved by the Animal Ethics Committee (IACUC project number I00319). An established *in vivo* porcine burn model (CBSET study number TV00008, approved by IACUC project number I00319) was used to assess the healing of cutaneous burns when treated with (1) hydrogel **6** as compared to standard of care dressings including (2) sterile gauze, (3) Mepilex™, and (4) Xeroform (N = 3/treatment). Five female Yorkshire swine (69.0–74.5 kg) were burned at 80 °C, for 20 s with a 4 cm diameter, 2 kg brass cylinder. Each pig received 12 four cm diameter burn wounds. This volume of burn covered most of the pig's back, and each pig received a burn area of 0.4% of their body surface area. Triple antibiotic ointment was applied to each burn sites prior to dressing treatment. Dressing changes and euthanize were performed at the designated time points for each group according to Fig. 5. Burn tissues were harvested and stained with H&E at 7- and 14-days post burn.

Necrosis and neovascularization scores were determined using the microscopic changes scoring matrix: 0 = no observable change; 1 = minimal – a nearly imperceptible feature/change, 2 = mild/moderate – an easily identifiable and/or notable feature/change in the tissue; 3 = marked/severe – prominent feature/change in the tissue. Scores were reported as mean ± standard deviation for each dressing in each group.

Individual histopathologic evaluation and hematoxalin & eosin staining are presented in Tables S1–S5 in ESI.† The Study Pathologist was blinded to the treatment matrix at the time of the pathologist read.

Conclusions

We have synthesized and characterized a small library of dissolvable hydrogels for use as burn wound dressings. We have demonstrated tunable mechanical strength, dissolution, swelling, and adhesion of these hydrogels based on the hydrogel composition. Specifically, the hydrogel prepared from PEI and crosslinker **6**: (1) is stable for over 7 days, (2) can be applied *in situ* to a burn site, (3) adheres to the tissue, (4) exhibits strength on the same order as human skin, (4) is dissolvable in under 30 minutes for atraumatic removal; and, (5) is efficacious in an *in vivo* burn model. This work highlights the tunability of hydrogels utilizing different methylene chain lengths within the NHS activated PEG crosslinker, the concept of *in situ* hydrogel formation and dissolution, and their successful application as burn wound dressings in a large animal model.

Author contributions

Katherine A. Cook, Nada Naguib, Jack Kirsch, Katherine Hohl, and Aaron H. Colby performed the experiments. Katherine A. Cook, Jack Kirsch and Katherine Hohl analyzed the data. Katherine A. Cook wrote the manuscript with comments and edits by Edward K. Rodriguez, Ara Nazarian, Rob Sheridan, and Mark W. Grinstaff.

Conflicts of interest

The authors declare a conflict of interest. K.A.C., A.H.C., and M.W.G. are listed as a co-inventors on patents describing this technology and M.W.G. and A.H.C. are equity holders in Ionic Pharmaceuticals which is pursuing a license for the technology with BU.

Acknowledgements

We thank the NIH for funding this research (R01EB021308) and the Small Business Innovation Research (SBIR) program (R43 GM125412). We also thank Dr Benjy Cooper and CBSet for their assistance with the animal work, and Dr Conor Evans laboratory at Massachusetts General Hospital for providing skin samples for the adhesion tests.

References

1 C. Mock, M. Peck, M. Peden, E. Krug, R. Ahuja, H. Albertyn, W. Bodha, P. Cassan, W. Godakumbura, G. Lo, J. Partridge and T. Potokar, Burns, https://www.who.int/news-room/fact-sheets/detail/burns.
2 D. Church, S. Elsayed, O. Reid, B. Winston and R. Lindsay, *Clin. Microbiol. Rev.*, 2006, **19**, 403–434.
3 N. E. Atchison, F. Osgood, D. B. Carr and K. Szyfelbein, *Pain*, 1991, **47**, 41–45.
4 T. Beushausen and K. Mücke, *Int. Pediatr. Surg.*, 1997, 327–333.
5 K. Judkins, *Pain Rev.*, 1998, 1998.
6 M. Peck, J. Molnar and D. Swart, *Bull. W. H. O.*, 2009, **87**, 802–803.
7 G. Iv, Management of Burns, https://www.who.int/surgery/publications/Burns_management.pdf.
8 J. Wasiak and H. Cleland, *Clin. Evid.*, 2015, 1–44.
9 J. L. Daristotle, L. W. Lau, M. Erdi, J. Hunter, A. Djoum, J. Priya, S. Xiaofang, W. Mousumi, O. B. Ayyub, A. D. Sandler and P. Kofinas, *Bioeng. Transl. Med.*, 2020, 1–12.
10 M. Latarjetl and J. Choinere, *Burns*, 1995, **21**, 344–348.
11 K. Duchowny, *J. Burn Care Res.*, 2020, **40**, 2008–2010.
12 G. Jozsa, P. Vajda, A. Garami, A. Csenkey and Z. Juhasz, *Medicine (Baltimore)*, 2018, **97**, e9991.
13 D. E. Fullenkamp, J. G. Rivera, Y. K. Gong, K. H. A. Lau, L. He, R. Varshney and P. B. Messersmith, *Biomaterials*, 2012, **33**, 3783–3791.
14 D. Queen, J. H. Evans, J. D. S. Gaylor, J. M. Courtney and W. H. Reid, *Burns*, 1987, **13**, 218–228.
15 M. Gandhi, C. Thomson, D. Lord and S. Enoch, *Int. J. Pediatr.*, 2010, **2010**, 825657.
16 Y. Loo, Y. Wong, E. Z. Cai, C. Ang, A. Raju, A. Lakshmanan, A. G. Koh, H. J. Zhou, T. Lim, S. M. Moochhala and C. A. E. Hauser, *Biomaterials*, 2014, **35**, 4805–4814.
17 J. M. Campbell, S. Kavanagh, R. Kurmis and Z. M. MClinSci, *J. Burn Care Res.*, 2017, **38**, 552–567.
18 M. D. Konieczynska, J. C. Villa-Camacho, C. Ghobril, M. Perez-Viloria, K. M. Tevis, W. A. Blessing, A. Nazarian, E. K. Rodriguez and M. W. Grinstaff, *Angew. Chem., Int. Ed.*, 2016, **55**, 9984–9987.
19 J. K. Wright, J. Kalns, E. a. Wolf, F. Traweek, S. Schwarz, C. K. Loeffler, W. Snyder, L. D. Yantis and J. Eggers, *J. Trauma*, 2004, **57**, 224–230.
20 A. M. Oelker, J. A. Berlin, M. Wathier and M. W. Grinstaff, *Biomacromolecules*, 2011, **12**, 1658–1665.
21 C. J. Hawker and K. L. Wooley, *Science*, 2005, **309**, 1200–1206.
22 H. Watabe, Y. Yamaji, M. Okamoto, S. Kondo, M. Ohta, T. Ikenoue, J. Kato, G. Togo, M. Matsumura, H. Yoshida,

T. Kawabe and M. Omata, *World J. Gastrointest. Endosc.*, 2006, **64**, 73–78.
23 E. A. Kamoun, E. R. S. Kenawy and X. Chen, *J. Adv. Res.*, 2017, **8**, 217–233.
24 B. Stubbe, A. Mignon, H. Declercq, S. Van Vlierberghe and P. Dubruel, *Macromol. Biosci.*, 2019, **19**, 1–12.
25 M. J. Zohuriaan-Mehr, H. Omidian, S. Doroudiani and K. Kabiri, *J. Mater. Sci.*, 2010, **45**, 5711–5735.
26 M. D. Konieczynska and M. W. Grinstaff, *Acc. Chem. Res.*, 2017, **50**, 151–160.
27 S. Tang, B. M. Richardson and K. S. Anseth, *Prog. Mater. Sci.*, 2020, 100738.
28 W. Huang, Y. Wang, Z. Huang, X. Wang, L. Chen, Y. Zhang and L. Zhang, *ACS Appl. Mater. Interfaces*, 2018, **10**, 41076–41088.
29 K. Y. Lee and D. J. Mooney, *Chem. Rev.*, 2001, **101**, 1869–1880.
30 A. Singh, P. K. Sharma, V. K. Garg and G. Garg, *Int. J. Pharm. Sci. Rev. Res.*, 2010, **4**, 97–105.
31 J. Zhu and R. E. Marchant, *Expert Rev. Med. Devices*, 2011, **8**, 607–626.
32 R. C. Op't Veld, X. F. Walboomers, J. A. Jansen and F. A. D. T. G. Wagener, *Tissue Eng., Part B*, 2020, **26**, 230–248.
33 S. Cascone and G. Lamberti, *Int. J. Pharm.*, 2020, **573**, 118803.
34 Y. Zhao, Z. Li, Q. Li, L. Yang, H. Liu, R. Yan, L. Xiao, H. Liu, J. Wang, B. Yang and Q. Lin, *Macromol. Rapid Commun.*, 2020, **2000441**, 1–11.
35 C. Ghobril, K. Charoen, E. K. Rodriguez, A. Nazarian and M. W. Grinstaff, *Angew. Chem., Int. Ed.*, 2013, **52**, 14070–14074.
36 C. Pailler-mattei, S. Bec and H. Zahouani, *Med. Eng. Phys.*, 2008, **30**, 599–606.
37 C. Ghobril and M. W. Grinstaff, *Chem. Soc. Rev.*, 2015, **44**, 1820–1835.
38 S. A. Burke, M. Ritter-Jones, B. P. Lee and P. B. Messersmith, *Biomed. Mater.*, 2007, **2**, 203–210.